RESEARCH ACTIVITIES III
Department of Electronic Structure

III-A Photochemical Synthesis of Exotic Atomic-Molecular Binary Clusters in Solution: π Radical -Transition Metal Alternatively Stacking $(\pi\text{–}d)_n$ Clusters

We have started the bulk synthesis of atom-molecule alternatively stacking clusters in solution. Originally, unpaired electrons are located in every atoms and molecules to induce strong interaction among *d* electrons in atoms and π electrons in molecules. Strong coupling of π and *d* electrons is shown by ab initio molecular orbital calculations of $(C_5H_5)V(C_5H_5)V(C_5H_5)V(C_5H_5)$ making inter-atomic and intermolecular distances short. Structural isomers are expected to appear for the clusters expressed by $((C_5H_5)V)_n$ and $((C_5H_5)V)_n(C_5H_5)$. One is cyclic the other is linear. For the analysis of the solid samples soluble in some specific solvents, we have developed a new mass spectrometer with a liquid jet nozzle, a rotating titanium drum for spiral adsorption of the sample on the surface, and a reflectron time-of-flight mass spectrometer situated in a separated high vacuum chamber. Thus we can mass-analyze the synthesized product directly from the solutions.

III-A-1 π Radical-Transition Metal Alternatively Stacking $(\pi\text{–}d)_n\text{–}\pi$ Clusters: (I) $V_6(C_5H_5)_7$, a Pentagonal Ring $((C_5H_5)V)$ with a Rolling Axis Vanadocene $(C_5H_5)V(C_5H_5)$?

HINO, Kazuyuki[1]; INOKUCHI, Yoshiya; NISHI, Nobuyuki
([1]Kyushu Univ.)

Photochemical treatment of the mixtures of vanadocene (bis(η–cyclopentadienyl) vanadium $((C_5H_5)V(C_5H_5))$ and tetracarbonyl (η–cyclopentadienyl) vanadium $((CO)_4V(C_5H_5))$ in dichloromethane produced the clusters with the compositions of $((C_5H_5)V)_n$ and $((C_5H_5)V)_n(C_5H_5)$ as well as $((C_5H_5)V)_n(C_5H_5)_2$. The product ratio varied with the changes of the ratio of the raw materials and the irradiation time. Addition of tricarbonyl (η–cyclopentadienyl) manganese enhanced the yields of these three kinds of clusters free from contamination of manganese in the clusters. Figure 1 shows the mass spectra of the photoproducts soluble in methanol. Starting from $((CO)_4V(C_5H_5))$, the photolysis produced vanadocene: (m/Z = 181) and $(C_5H_5)_2$: (m/Z = 130). This indicates that C_5H_5 is also dissociated by electronic excitation as well as the CO groups from the carbonyl compound. Addition of vanadocene as a raw material vanishes the signal of vanadocene but produces a new product at m/Z = 503. The main high mass product is found at m/Z = 761. This product is observed in any system with either the carbonyl compound or vanadocene. Therefore we assign this signal to $((C_5H_5)V)_6(C_5H_5)$. This compound must be much more stable than the linear polymer expressed by the same formula, since there is no reason for such a linear cluster to show specific high stability at n = 6. A possible structure for this cluster is shown at the upper right of Figure 1, that has a vanadocene molecule $((C_5H_5)V(C_5H_5))$ vertically inserted in a pentagonal ring $((C_5H_5)V)_5$. The pentagonal ring has 50 electrons ($4 \times 12 + 2$) distributed in the valence orbitals composed of 3*d* and 3*s* atomic orbitals of vanadium and π orbitals of cyclopentadienyl. The ring may act as a wheel rotating around the axle vanadocene. DFT calculation of this compound is now going on to check the stability of this form. The clusters are stable in alcohol solutions or in vacuum but not so stable in air.

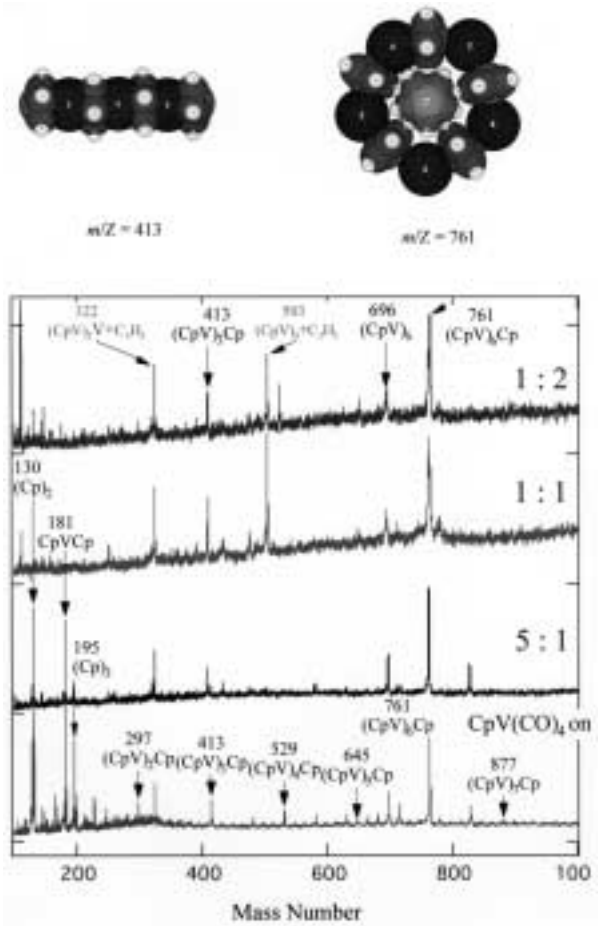

Figure 1. Mass spectra of the photoproducts from the solutions with various mixing ratio of $((CO)_4V(C_5H_5))$ to $(C_5H_5)V(C_5H_5)$.

III-A-2 Development of a New Mass Spectrometer Allowing the Injection of Solution Directly into Vacuum and the Desolvation through the Collision of Liquid Jet with Solvent Gas Flow Rebounded from a Rotating Titanium Drum for Solute Deposition

INOKUCHI, Yoshiya; HINO, Kazuyuki[1]; NISHI, Nobuyuki
([1]Kyushu Univ.)

Mass spectrometry is a very powerful method for determining mass numbers of unknown samples and getting information on molecular structures. We have developed a new mass spectrometer for non-volatile samples. Figure 1(a) shows a schematic diagram of the apparatus. It consists of a liquid beam source, a titanium drum, and a time-of-flight mass spectrometer. Non-volatile samples are dissolved in suitable solvents. Sample solutions are injected through a modified injector needle into the vacuum chamber as a liquid beam. The outer surface of the rotating titanium drum is located at 5 mm away from the exit of the needle. The liquid beam collides with gaseous shock front of the scattered solvent at the drum surface. The solvent is vaporized, and only the solute is fixed as a spiral deposit on the drum. The drum rotates at 1 rpm. The spiral solid deposit line is irradiated by the third harmonics of a Nd:YAG laser (355 nm) introduced through a hole between a sample chamber and a main chamber situated with an ion optics of the mass spectrometer. The produced ions detached from the surface are mass-analyzed by the time-of-flight mass spectrometer with a reflectron. Since the non-volatile samples are directly introduced into the spectrometer as solutions and fixed as a spiral line on the drum, we can measure the mass spectra of the non-volatile samples without exposing them to the air. Figure 1(b) represents mass spectra of polyethylene glycols used for mass calibration. Both spectra show ion signals with uniform interval of m/z = 44. This system is used for the product analysis of the synthesis of $(\pi\text{-}d)_n$ clusters.

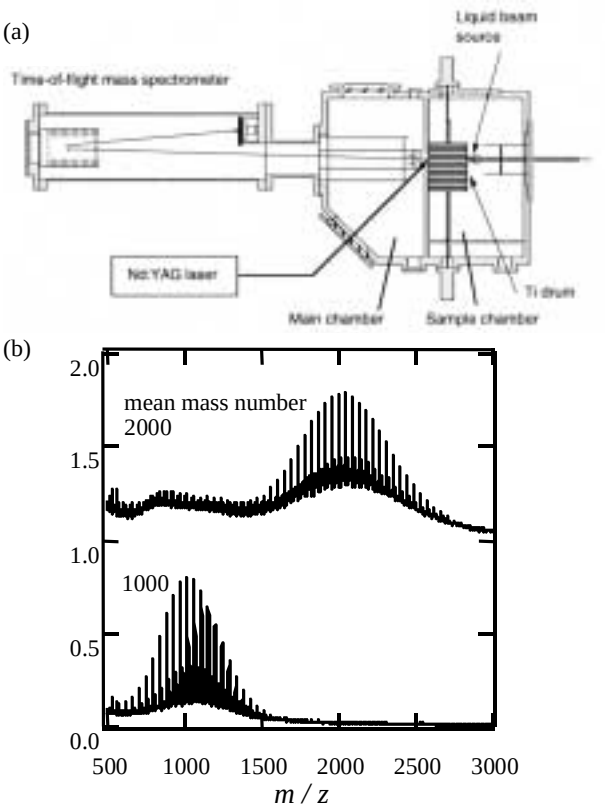

Figure 1. (a) a schematic diagram of the apparatus, (b) mass spectra of polyethylene glycol polymer samples with a mean mass number 2000 (top) and 1000(bottom).

III-B States of Neutral and Ionic Molecular Associates in Solutions

States of molecular associates particularly in aqueous solutions are of great importance in understanding the role of molecules in living organisms. Our recent studies of low frequency Raman spectroscopy of binary aqueous solutions of alcohols and carboxylic acids have shown that these amphiphilic molecules form "microphases" of clusters with the same solute species (*J. Phys Chem.* **102**, 4054 (1998), *J. Phys. Chem. A* **103**, 10851 (1999)). We have extended these studies from both experimental and theoretical point of view.

III-B-1 Monomeric and Cluster States of Acetic Acid Molecules in Solutions: A Raman Spectroscopic Study

NAKABAYASHI, Takakazu; NISHI, Nobuyuki

The purpose of this study is to understand on a microscopic scale about local structures of acetic acid in the liquid and solution states. Since acetic acid has both the hydrogen donor and acceptor sites in a molecule, various kinds of associations of acetic acid molecules can be expected depending on the situation. As shown in Figure 1, acetic acid forms a cyclic dimer in the gas phase, polymer chains in the crystalline state, and the chain clusters as the fragments of the crystalline networks in the liquid state.[1)] In aqueous solution, we have recently suggested that acetic acid preferentially forms microphase aggregates in which the side-on dimer structure is an elementary unit.[2)] In other words, two microphases exist in acetic acid-water binary solutions: one is water rich phase and the other is acetic acid one. What should be discussed next is whether the acetic acid microphases exist in other solvents or not. To examine this point, we have observed Raman spectra of acetic acid in alcohols and aprotic solvents with varying mole fraction of acetic acid (χ_{AA}). Raman spectra of acetic acid in the C=O stretching region are shown in Figure 2. With the addition of water into

liquid acetic acid, the C=O band broadens and shifts to a higher wavenumber, which is ascribed to the generation of the side-on dimer microphases.[2] In alcohols, the C=O band also shifts to a higher wavenumber and the resultant peak position is the same as that observed in water. This result suggests that the side-on dimer microphases also exist in alcohols. Low-frequency Raman spectra also support the above conclusion. In dipolar aprotic solvents such as acetonitrile, however, the spectral shift was apparently different from that in protic solvents: two prominent Raman bands appear on the higher-wavenumber side of the C=O bands observed in protic solvents. Analyses of the temperature and concentration dependencies of the Raman spectra suggest the generation of monomeric acetic acid in dipolar aprotic solvents with dilution. From these results, it is concluded that the acetic acid molecules exist as the microphases in protic solvents and as the monomeric molecules in dipolar aprotic solvents as depicted in Figure 1.

References

1) T. Nakabayashi, K. Kosugi and N. Nishi, *J. Phys. Chem. A* **103**, 8595 (1999).
2) N. Nishi, T. Nakabayashi and K. Kosugi, *J. Phys. Chem. A* **103**, 10851 (1999).

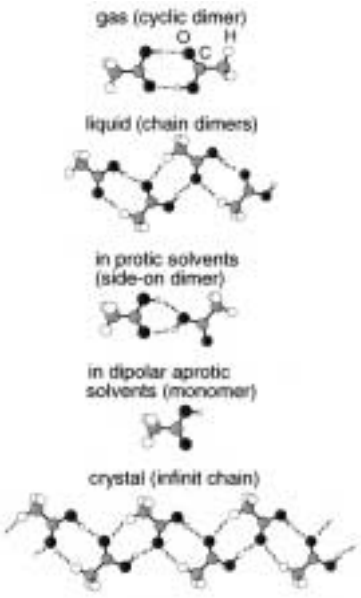

Figure 1. Structures of acetic acid clusters in various situations.

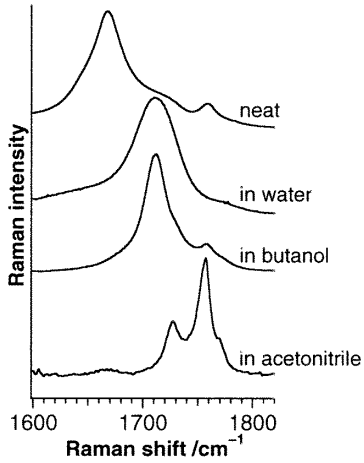

Figure 2. Raman spectra of acetic acid in the C=O stretching region (χ_{AA} = 0.015).

III-B-2 Comparison of the Theoretical Models for Calculating Acetic Acid Clusters in Aqueous Solution

NAKABAYASHI, Takakazu; SATO, Hirofumi; HIRATA, Fumio; NISHI, Nobuyuki

There has been tremendous progress in the theories for calculating molecular properties in solutions. In the present study, we have applied the SCRF and the RISM-SCF methods to clarify the electronic structures of acetic acid clusters in aqueous solution. In the SCRF method, the solute occupies a cavity surrounded by the dielectric continuous solvent. A solute dipole and/or multipole will induce a reaction field, which in turn will act to stabilize the solute. We applied the simplest SCRF model that makes use of a spherical cavity and considers only the solute dipole. The RISM-SCF method is an ab initio self-consistent field method combined with an extended version of the reference interaction site method. The advantage of the RISM-SCF method is to maintain the molecular aspects of solvents and thus to describe local interactions such as hydrogen bonds. Table 1 shows the calculated binding energies of acetic acid dimers (the linear dimer structure is depicted in Figure 1). In the gas phase, the cyclic dimer is the most stable among acetic acid dimers. Force calculations for the cyclic and side-on dimers confirm convergence to the minima on the energy surface, while the linear dimer is optimized to be a saddle point. In aqueous solution, owing to the stabilization in the side-on dimer, the energy difference between the cyclic and side-on dimers is calculated to be reduced by the RISM-SCF method; 3.0 kcal/mol in the solution compared with 8.1 kcal/mol in the gas phase. Decomposition of the solvation energy indicates that the hydration around the free carbonyl oxygen is of great importance for lowering the total energy of the side-on dimer. Marked stabilization is also obtained in the linear dimer. Not only solvation around the free carbonyl oxygen but also the increase in the O–H··O=C hydrogen bond contributes the stabilization in the linear dimer, although the free hydroxyl group has only a minor effect on the solvation energy. From the RISM-SCF results, the cyclic and linear dimer structures as

well as the side-on dimer one are suggested in aqueous solution, although force calculations under the RISM-SCF model are needed to discuss whether the linear dimer is at the energy minimum in aqueous solution or not. In the case of the SCRF method, the binding energies in aqueous solution for the cyclic, side-on and linear dimers are calculated to be –12.86, –6.79, and –6.05 kcal/mol, respectively. This result indicates that, within the limits of the electrostatic interactions at the dipole level, the cyclic dimer is fairly stable even in aqueous solution. The SCRF model predicts that the energy difference between the side-on and linear dimers remains almost unchanged on going from the gas phase to aqueous solution, which is also different from the RISM-SCF result.

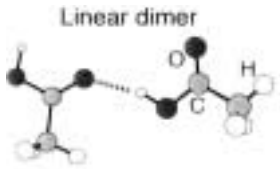

Figure 1. Chemical structure of the linear dimer.

	Gas	Solution	
		RISM	SCRF
Cyclic	–14.37	–1.32	–12.86
Side-on	–6.25	1.68	–6.79
Linear	–5.55	0.32	–6.05

Table 1. Binding Energies (in kcal/mol) of Acetic Acid Dimers in Gaseous phase and Aqueous Solution at the HF/DZP Level.

III-C Ultrafast Dynamics and Structural Changes of Excited Cation Radicals in Solution

Dynamic behavior and structural change of ion molecules generated in liquid solution, particularly in the presence of electron donor or acceptor species, are of great interest in relation to the formation of complexes as reaction intermediates. As an initiating stage, we have studied photogeneration of aromatic radical cations in polar solvents for understanding ion stabilization and destabilization processes in solution.

III-C-1 First Observation of the Formation Process of a Solvated Aromatic Cation Radical in Polar Solvents: A Two-Photon Pumped Femtosecond Time-Resolved Absorption Study

KAMO, Satoshi[1]; NAKABAYASHI, Takakazu; WATANABE, Kazuo; SAKURAGI, Hirochika[1]; NISHI, Nobuyuki
([1]Univ. Tsukuba and IMS)

Multiple-photoionization of aromatic compounds has been studied extensively in view of its importance in photochemical and photobiological primary processes. Photoionization in condensed phase is considered to be characterized by the production of a solvent-separated electron-cation ion pair. In polar solvents, the resultant charges can be stabilized by the polarization of the solvent and then solvated free cation radicals are produced efficiently. However, direct observations of the formation of the solvated free ion are still lacking. In order to clarify the details of multiple-photoionization process, therefore, we first observed the ultrafast dynamics of the naphthalene cation radical by using two-color two-photon pumped femtosecond time-resolved absorption spectrometer. The neutral naphthalene molecules were excited to the S_1 state by the first pump photon at 267 nm. After 100 ps, the S_1 molecules were excited by the second pump photon at 400 nm through the $S_n \leftarrow S_1$ absorption, producing the naphthalene cation radical. The absorption changes induced by the two-color two-photon pump pulses were probed by a white light continuum with the time resolution of ≈300 fs. Figure 1A shows the transient absorption spectra of naphthalene in ethyl acetate in the delay time of 600 fs–24 ps from the second pump pulse. The transient absorption observed at 600 fs exhibits two broad peaks around 660 and 710 nm. This absorption signal decreases in several picoseconds and the new absorption with peaks around 660 and 690 nm appears at 15 and 24 ps. The spectral profile of the latter absorption changes from a broad one to a sharp one as seen in Figure 1B, indicating that the absorption appeared at 15 and 24 ps arises from the vibrationally hot solvated naphthalene cation radical. The absorption observed at 600 fs is ascribable to its precursor. Almost the same spectral changes are observed in acetonitrile in Figure 2A, although the absorption signal at 600 fs is ≈1.8 times larger in acetonitrile than in ethyl acetate. This suggests that the yield of the solvated cation radical is determined within 600 fs. As shown in Figures 1B and 2B, the peak intensity in acetonitrile rises with a time constant of tens of picoseconds, while that in ethyl acetate remains almost unchanged. This result appears to be consistent with the picosecond Raman study (in the next subsection) suggesting that the Raman intensity change in acetonitrile arises from the fluctuation of the solvation structure due to vibrational relaxation.

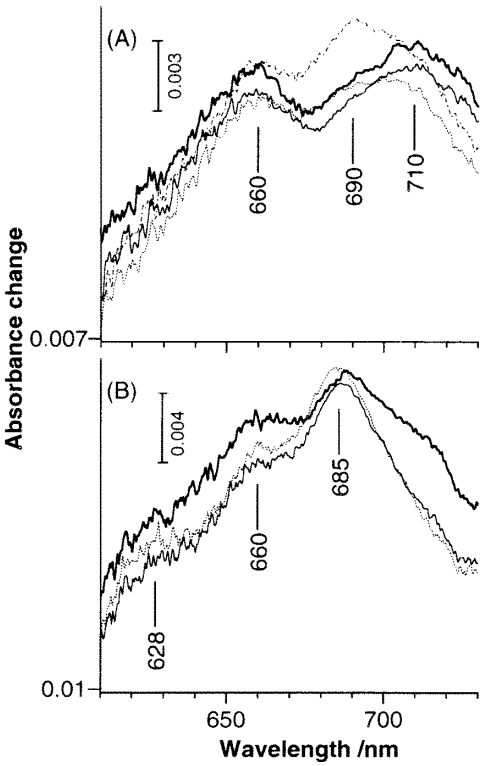

Figure 1. Transient absorption spectra of naphthalene in acetonitrile. (A) Thick-solid line, 600 fs; thin-solid line, 2 ps; dotted line, 15 ps; dash-dotted line, 24 ps. (B) Thick-solid line, 35 ps; thin-solid line, 65 ps; dotted line, 145 ps.

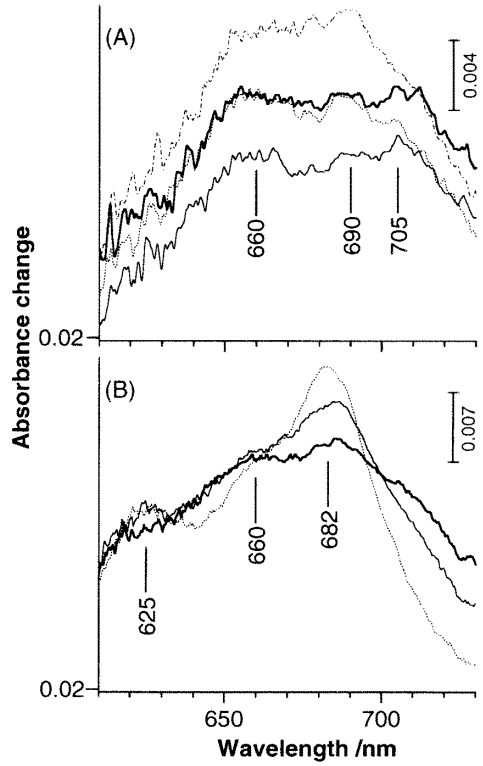

Figure 2. Transient absorption spectra of naphthalene in ethyl acetate. (A) Thick-solid line, 600 fs; thin-solid line, 2 ps; dotted line, 15 ps; dash-dotted line, 24 ps. (B) Thick-solid line, 35 ps; thin-solid line, 65 ps; dotted line, 145 ps.

III-C-2 Vibrational Relaxation Process of Solvated Aromatic Cation Radicals in Polar Solvents: A Two-Photon Pumped Picosecond Time-Resolved Raman Study

NAKABAYASHI, Takakazu; KAMO, Satoshi[1]; SAKURAGI, Hirochika[1]; NISHI, Nobuyuki
([1]Univ. Tsukuba and IMS)

Time-resolved Raman spectroscopy is already well recognized as a powerful technique for studying the structure and dynamics of short lived species in solution. To our knowledge, however, no one has reported picosecond Raman spectra of aromatic cation radicals, primarily because of the difficulty in obtaining two color picosecond pulses with sufficient pulse energies. Recently, we have constructed a two independently tunable Raman spectrometer with the time resolution of 3 ps. By using this system, we have first measured picosecond Raman spectra of aromatic cation radicals (biphenyl, trans-stilbene and naphthalene) in polar solvents. The results for biphenyl in ethyl acetate and acetonitrile are shown in Figure 1. Resonance Raman bands due to the S_1 state and cation radical of biphenyl are observed in this figure. The laser power dependencies confirm that the cation radical is produced through a two photon process. The frequencies of cation bands as well as their bandwidths change with the delay time in both the solvents. Immediately after biphotonic ionization, vibrationally excited cation radicals should be generated because of a large amount of excess vibrational energy. Thus the spectral changes can be ascribed to vibrational relaxation of the cation radical toward a thermal equilibrium with solvents. The time constant of the positional change of the 1610 cm^{-1} cation band is estimated to be 17 ps in acetonitrile and 13 ps in ethyl acetate. The obtained constants are roughly the same as those of other neutral aromatic molecules reported so far, although the interactions between the cation radical and surrounding solvents can be expected to be large. This result therefore supports the very rapid cooling model that the ultrafast energy transfer to the nearest solvent shell first occurs and then the energy flow into the bulk solvent follows in tens of picoseconds. As shown in Figures 1A and 2A, both the Raman intensities arising from the S_1 and cation species show an instrumental-limited rise (< 3 ps) in weak polar solvents such as ethyl acetate. On the other hand, in highly polar solvents such as acetonitrile, the Raman intensities arising from the cation radical rise in tens of picoseconds, and reach their maxima at ≈40 ps (Figures 1B and 2B). Since the picosecond intensity rise only occurs in highly polar solvents forming strong solvent-solute interactions and its time constant is roughly the same as that of vibrational relaxation, it is conceivable that the energy transfer to solvents disturbs the solvation structure, which causes the intensity change in the cation Raman bands.

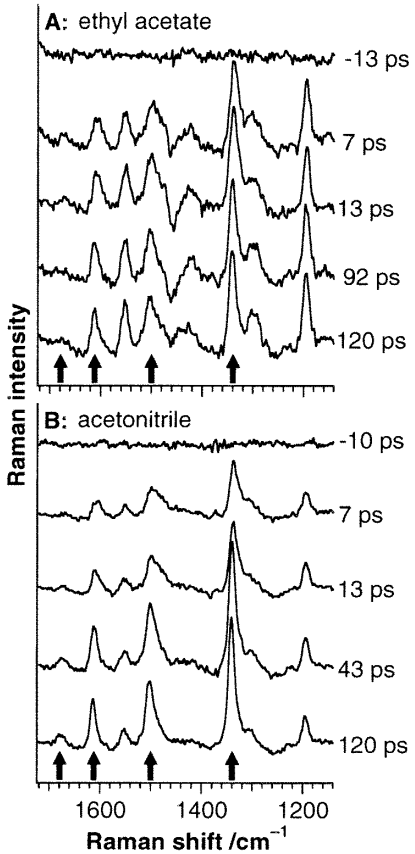

Figure 1. Picosecond time-resolved Raman spectra of biphenyl. Arrows indicates Raman bands due to the cation radical of biphenyl. Pump: 262 nm, probe: 633 nm. The Raman bands of the solvents are subtracted.

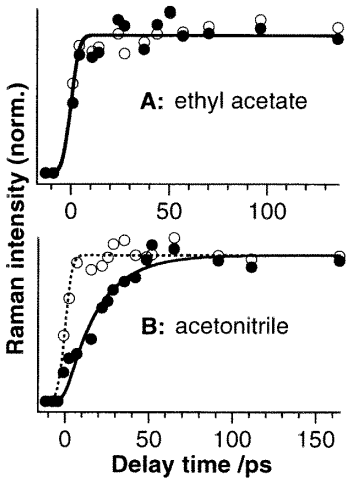

Figure 2. Plot of the transient Raman intensities against the delay time. Blank circles, S_1 (1195 cm^{-1}); filled circles, cation (1340 cm^{-1}).

III-D Spectroscopic and Dynamical Studies on Charge Delocalization and Charge Transfer in Aromatic Molecular Cluster Ions

Electron deficiency of aromatic molecular cations can attract electron rich groups or atoms exhibiting charge resonance(CR) interaction between similar molecules or charge transfer (CT) interaction with electron donor molecules. Here we show intersting cases of benzene cation complexes and clusters.

III-D-1 Photodissociation Spectroscopy of Benzene Cluster Ions in Ultraviolet and Infrared Regions. Static and Dynamic Behavior of Positive Charge in Cluster Ions

INOKUCHI, Yoshiya; NISHI, Nobuyuki

[*J. Chem. Phys.* submitted]

Photodissociation spectroscopy is applied to benzene cluster ions in ultraviolet and infrared regions. In the ultraviolet photodissociation spectrum of $(C_6H_6)_3^+$, a characteristic broad band emerges at 255 nm. This band is assigned to a $\pi^* \leftarrow \pi$ transition of a solvent benzene molecule that exists in the trimer. On the basis of the ultraviolet and the previous near-infrared spectra, we confirm a dimer ion core structure of $(C_6H_6)_3^+$; there are a dimer ion core and the solvent benzene molecule in $(C_6H_6)_3^+$. Figure 1 shows infrared photodissociation spectra of $(C_6H_6)_n^+$ (n = 3–5) (open circles). The spectra clearly show a sharp band at 3066 cm^{-1}. The band is attributed to a C–H stretching vibration of the dimer ion core. The infrared spectra can be reproduced by combining the C–H stretching bands of the dimer ion core and the solvent benzene molecules. The infrared photodissociation spectra of mixed benzene trimer ions with one or two benzene-d_6 molecules demonstrate that there is no correlation between the excited dimer ion core site in the trimer and the photofragment dimer ion species. This implies that a dimer ion core switching, in other words, a charge hopping occurs in photoexcited vibrational states prior to the dissociation. The charge hopping in cluster ions is thought to be a simple example of the charge transportation in condensed

phases.

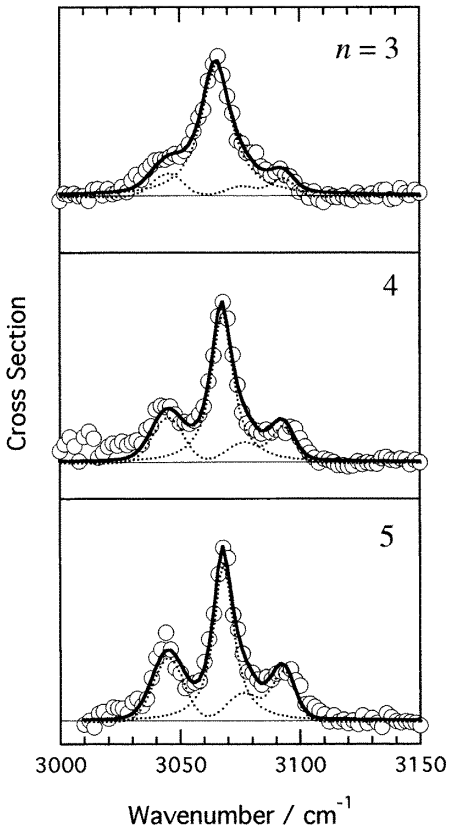

Figure 1. Infrared photodissociation spectra of $(C_6H_6)_n^+$ (n = 3–5).

III-D-2 Charge Transfer Complex of Benzene Cation Vertically Coordinated with Acetic Acid

KOSUGI, Kentaroh; INOKUCHI, Yoshiya; NISHI, Nobuyuki

[*J. Chem. Phys.* in press]

The non-bonding orbital on the oxygen atom of carboxyl group can take a role of strong electron donor for a cationic molecule. Benzene cation is a good electron acceptor molecule as a counter-part of the acetic acid. We have measured vibrational and electronic spectra of acetic acid-benzene cation complexes through ion-trap photodissociation spectroscopy. Ab initio molecular orbital calculation at CASSCF(7,7)/6-31G** level for the analysis of the electronic spectrum and at B3LYP/6-31G** level for the vibrational spectrum demonstrated that there are two or three isomers: charge transfer complex with an acetic acid sitting on a carbon atom of the benzene cation vertically to the ring (vertical isomer V), and in-plane complexes with a cis- or trans- acetic acid hydrogen-bonded to one or two hydrogen atom(s) of the benzene C-H groups (horizontal isomers H). The charge transfer complex shows very broad bands due to charge transfer electronic transitions in near infrared and visible region as seen in Figure 1, where one can see the optimized structure of the vertical complex and the intermolecular bonding and anti-bonding molecular orbitals involved in the electronic transitions. One can see the negative charge in the acetic acid is transferred to the benzene on the electronic transition indicated by V_2.

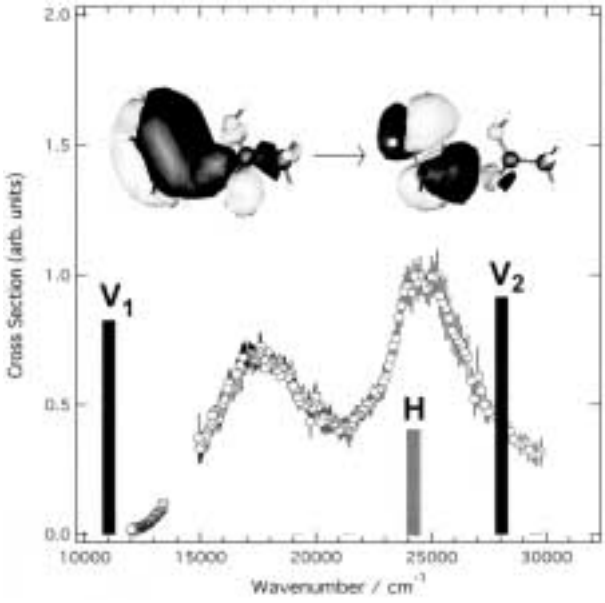

Figure 1. Observed photodissociation spectrum of $(CH_3COOH)(C_6H_6)^+$ and the transition energies and oscillator strengths calculated by the MCQDPT method.

III-D-3 Vibrational and Electronic Spectra of (Benzene-Benzyl Alcohol)$^+$; Predominance of Charge Resonance Interaction over Hydrogen-Bonding Interaction

OHASHI, Kazuhiko[1]; IZUTSU, Hironobu[1]; INOKUCHI, Yoshiya; HINO, Kazuyuki[1]; NISHI, Nobuyuki; SEKIYA, Hiroshi[1]
([1]Kyushu Univ.)

[*Chem. Phys. Lett.* **321**, 406 (2000)]

Vibrational and electronic spectra of the benzene-benzyl alcohol hetero-dimer ion are measured by photodissociation spectroscopy. The vibrational spectrum shows a prominent band at 3662 ± 3 cm^{-1}, which is assigned to the stretching vibration of the OH group free from intermolecular perturbations. The electronic spectrum shows a broad band around 950 nm, which arises from a charge resonance interaction between the aromatic rings. These results suggest that the ion has a sandwich-like structure suitable for the resonance interaction, without the hydrogen bond between the OH group of benzyl alcohol and the - electrons of benzene.

III-D-4 Electronic and Vibrational Spectra of Aniline-Benzene Hetero-Dimer and Aniline Homo-Dimer Ions

OHASHI, Kazuhiko[1]; INOKUCHI, Yoshiya; IZUTSU, Hironobu[1]; HINO, Kazuyuki[1]; YAMAMOTO, Norifumi[1]; NISHI, Nobuyuki; SEKIYA, Hiroshi[1]
([1]Kyushu Univ.)

[*Chem. Phys. Lett.* **323**, 43 (2000)]

Structures of (aniline-benzene)$^+$ and (aniline)$_2^+$ are re-investigated by electronic spectroscopy in the near-infrared region and vibrational spectroscopy in the NH stretching region. The spectra of (aniline-benzene)$^+$ indicate a structure including a hydrogen bond between an NH bond of the ionic aniline and the -electrons of the neutral benzene. Two isomers are suggested for (aniline)$_2^+$ in which an NH bond of the ionic aniline forms different types of hydrogen bond with the neutral aniline: one with the -electrons of the aromatic ring and the other with the lone pair of the nitrogen atom.

III-E Structures and Reactivities of Metal Clusters

Clusters of metal atoms constitute a new class of material whose properties deviate significantly from those of isolated atoms and condensed matters. Our research group, started in January 2000, has been developing an experimental setup to study the size and shape dependent catalytic behavior of the metal clusters. The motivation of our research is to understand detailed mechanism of the chemical reactions involving the metal clusters based on the correlation with geometric/electronic structures.

III-E-1 Construction of Apparatus for Mass Analysis of Metal Clusters

NEGISHI, Yuichi; TSUKUDA, Tatsuya

We have designed a plan to exploit a synthetic method of the metal clusters having a well-defined size before studying the chemical reactivities. The metal cluster ions are prepared by reduction of the relevant metal ions in the presence of ionic surfactant molecules which prevent coalescence of the clusters. We have constructed a new apparatus that allows us to monitor mass distributions of the nascent clusters in liquid phase. Figure 1 shows a schematic diagram of the apparatus with 7 stages of differentially pumped vacuum chambers. The apparatus consists of an electrospray ion source and a reflectron time-of-flight (TOF) mass spectrometer. Liquid sample containing the cluster ions is pumped through a fused silica capillary, whose end is supported in a stainless steel needle. Charged aerosol droplets are electrosprayed by means of an electrical potential between the needle tip and a counterelectrode (+3–5 kV). The cluster ions in the droplets are evaporated into the gas phase and further desolvated by collision with an inert gas such as nitrogen. A portion of the ion flow is skimmed and introduced into the acceleration region of the TOF mass spectrometer. In order to increase the detection efficiency for the ions having a mass-to-charge ratio above ~10^4, the ions are accelerated by applying a pulsed output of 30 kV from a homemade pulse generator (rise time ~30 ns, on time ~200 μs). The ions are guided by several sets of ion optics and detected by microchannel plate located at the end of the flight path of 3.1 m. Surface induced dissociation, a powerful diagnostics for structural characterization of large and complex systems, can also be performed with this machine. Cluster ions of interest are mass-selected by pulsed beam deflectors and allowed to collide with a solid surface mounted at the end of the reflectron. Collision energy can be varied by changing the voltage applied to the surface. Secondary ions scattered off the surface are detected by secondary TOF mass spectrometer.

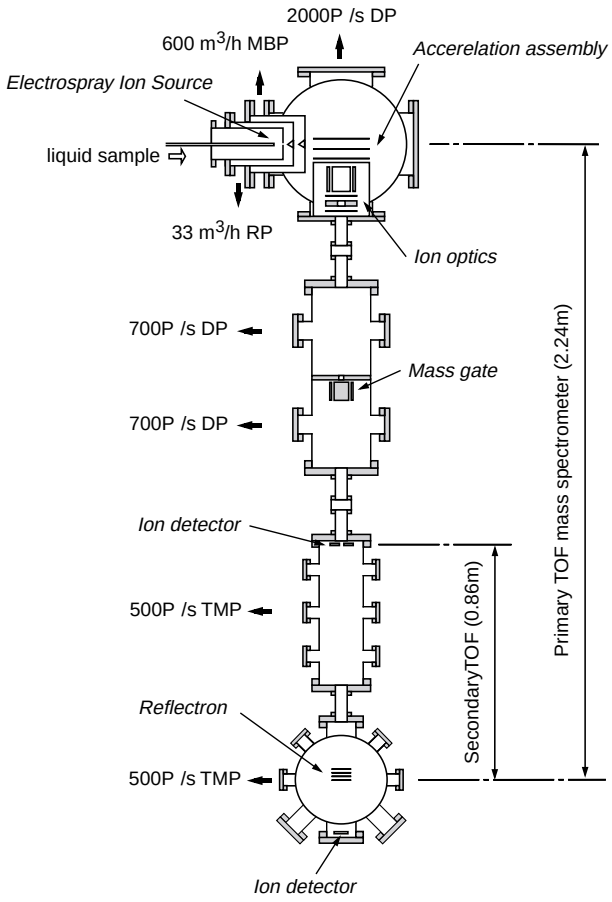

Figure 1. Schematic of experimental apparatus shown in cross section as viewed from above. RP: rotary pump; MBP: mechanical booster pump; DP: oil diffusion pump; TMP: turbo molecular pump.

III-F Spectroscopy and Dynamics of Vibrationally Excited Molecules and Clusters

This research group is studying structure and dynamics of molecules and clusters of in higher vibrational state by two-color double resonance spectroscopy. New spectroscopic methods will also be developed to observe the higher vibrational state under collision-free condition.

III-F-1 IR dip Spectra of Photochemical Reaction Products in a Phenol/Ammonia Cluster—Examination of Intracluster Hydrogen Transfer

ISHIUCHI, Shun-ichi[1]; SAEKI, Morihisa; SAKAI, Makoto; FUJII, Masaaki
([1]GUAS)

[*Chem. Phys. Lett.* **322**, 27 (2000)]

The vibrational transitions of the photochemical reaction products in phenol–$(NH_3)_3$ have been measured by IR dip spectroscopy. Two sharp bands at ~3200 cm^{-1} and a broad band in the region 2700~3100 cm^{-1} are observed. The spectrum is clearly different from that of the cluster in S_0, and also largely different from the IR spectrum of $NH_4^+(NH_3)_2$. This suggests that hydrogen transfer occurs in electronically excited phenol–$(NH_3)_3$. Evidence of hydrogen transfer has also been found in phenol–$(NH_3)_4$ based on the mass spectrum and the IR dip spectrum of the cluster.

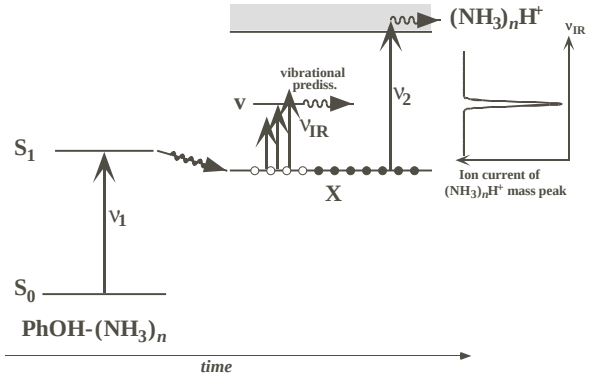

Figure 1. Schematic diagram showing the principle of IR dip spectroscopy which was employed in this work.

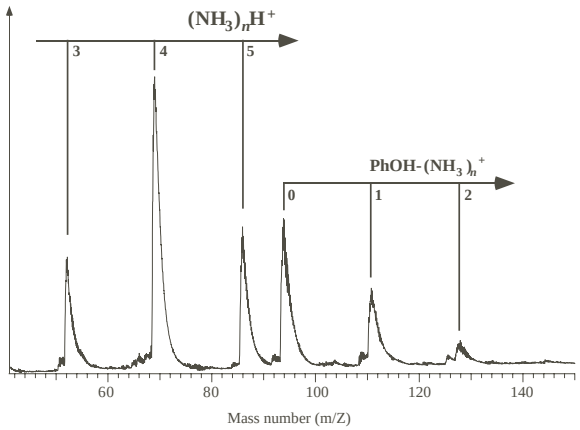

Figure 2. (a) IR dip spectrum of the reaction product which was observed by fixing ν_1 to the lower vibronic band in the S_1 state of PhOH–$(NH_3)_3$ (35498 cm^{-1}) and monitoring $(NH_3)_3H^+$. The third harmonics of the YAG laser was used as the ionization laser ν_2. Here, $(NH_3)_3H$ in the grand state can be ionized by one-photon of 355 nm light (IP = 3.31 eV). The IR laser ν_{IR} was irradiated after 180 ns from the excitation to S_1 due to ν_1. The solid curves and the dotted curves show the spectra obtained by adjusting the laser power of ν_{IR} to 0.2 mJ and 0.4 mJ, respectively. (b) IR dip spectrum of PhOH–$(NH_3)_3$ in S_0. The IR laser ν_{IR} was irradiated before 20 ns from the excitation to S_1 due to ν_1. All other conditions were the same as those for the IR dip spectrum of the reaction product (Figure 2a).

III-F-2 Structural Characterization of the Acridine–$(H_2O)_n$ (n = 1–3) Clusters by Fluorescence Dip Infrared Spectroscopy

MITSUI, Masaaki[1]; OHSHIMA, Yasuhiro[1]; ISHIUCHI, Shun-ichi[2]; SAKAI, Makoto; FUJII, Masaaki
([1]Kyoto Univ.; [2]GUAS)

[*Chem. Phys. Lett.* **317**, 211 (2000)]

Vibrational spectra of supersonically cooled acridine–$(H_2O)_n$ (n = 1–3) clusters in the electronic ground state have been measured by fluorescence dip infrared spectroscopy. The observed O–H stretching fundamentals of the solvents have been analyzed with the aid of density functional calculations, to assign structures of the clusters. In the n = 1 cluster, the water molecule acts as a proton donor which is hydrogen-bonded to the N atom of acridine. The second (third) water in the higher clusters is further hydrogen-bonded to the first (second) one to form a linear "water chain," which surrounds an edge of the acridine molecule approximately in the plane of the aromatic ring.

III-F-3 Internal Methyl Group Rotation in o-Cresol Studied by Pulsed Field Ionization-ZEKE Photoelectron Spectroscopy

SUZUKI, Kazunari[1]; EMURA, Yuji[2]; ISHIUCHI, Shun-ichi[3]; FUJII, Masaaki
([1]YAMAHA; [2]Mitsui Chemical; [3]GUAS)

[*J. Electron. Spectrosc.* in press]

Pulsed field ionization-ZEKE photoelectron spectroscopy and (1+1) R2PI spectroscopy have been applied to cis- and trans-o-cresol. The internal rotational structure in S_1 has been re-assigned for the cis-isomer, and the potential curve for the internal rotation has been determined. In the PFI-ZEKE spectra recorded via

different internal rotational levels in the S_1 state, well-resolved low-frequency bands have been observed. The low-frequency bands are assigned to internal rotational motion of the methyl group in the cation. Level energies and relative transition intensities are reproduced well by a one-dimensional rotor model with a three-fold axis potential. Potential curves for the internal rotation have been determined for both cis- and trans-o-cresol cations. The barrier height for the internal rotation is different for the two isomers in the cation, while it becomes similar in S_1. Contributions of steric and electronic factors to the rotational barrier are discussed.

III-F-4 Pulsed Field Ionization-ZEKE Spectroscopy of Cresoles and Their Aqueous Complex: Internal Rotation of Methyl Group and Intermolecular Vibrations

SUZUKI, Kazunari[1]; ISHIUCHI, Shun-ichi[2]; FUJII, Masaaki
([1]YAMAHA; [2]GUAS)

[*Faraday Discuss.* in press]

Pulsed field ionization-ZEKE photoelectron spectroscopy and (1+1) R2PI spectroscopy have been applied to cis- and trans-m-cresol·H_2O clusters. The internal rotational structure in S_1 has been re-assigned, and the potential curve has been determined for the cluster. The PFI-ZEKE spectra of cis- and trans-isomer show low-frequency bands up to 1000 cm^{-1} above the adiabatic ionization potential IP_0. The low-frequency bands are assigned to the internal rotation of the methyl group, the intermolecular stretching and their combination bands in the m-cresol·H_2O cluster cation. Level energies and relative transition intensities are reproduced well by a one-dimensional rotor model with a three-fold axis potential. Potential curves for the internal rotation have been determined for both cis- and trans-isomers of m-cresol·H_2O cations. The effect of the cluster formation upon the internal methyl rotation, and interaction between the methyl rotation and the intermolecular vibration are discussed.

III-F-5 Butterfly Vibration of the Tetrafluorobenzene Cation Studied by Pulsed Field Ionization-ZEKE Photoelectron Spectroscopy

TAKAZAWA, Ken[1]; FUJII, Masaaki
([1]Natl. Res. Inst. Met)

[*J. Electron. Spectrosc.* in press]

The pulsed field ionization-ZEKE photoelectron spectroscopy has been applied to 1,2,4,5-tetrafluorobenzene in a supersonic jet. The spectrum measured by selecting a specific vibronic level of butterfly vibrational mode in S_1 by the first laser shows well-resolved vibrational structure of the cation. A long progression has been assigned to the out-of-plane butterfly vibrational mode 11 with even quantum number in the cation. From the harmonisity and Franck-Condon factor, it has been concluded that the molecular structure of the tetrafluorobenzene cation is flat though that in S_1 is non-planer along the butterfly vibrational mode. The geometrical change upon ionization has been discussed in terms of the electronic structure.

III-G Time-Resolved Photoelectron Imaging on Ultrafast Chemical Dynamics

We have developed a novel experimental technique of time-resolved photoelectron imaging to probe excited state dynamics of isolated molecules and clusters in real time [*J. Chem. Phys.* **111**, 4859 (1999)]. A pump pulse prepares a non-stationary state in the excited electronic state, then a probe pulse projects the wavefunction to the cationic states. With a 1 kHz laser system, one electron image can be recorded for less than a minute, which allows us to map out excited state dynamics quite rapidly.

III-G-1 Femtosecond Time-Resolved Photoelectron Imaging on Ultrafast Dephasing in Pyrazine

TSUBOUCHI, Masaaki[1]; WHITAKER, Benjamin[2]; SUZUKI, Toshinori
([1]GUAS; [2]Univ. Leeds)

Femtosecond time-resolved photoelectron imaging was applied to ultrafast electronic dephasing in Pyrazine that is the best-known example of an intermediate coupling case in radiationless transition. A tunable pump pulse in 300 nm range prepared Pyrazine molecule in a variety of vibronic levels in $S_1(\pi,\pi^*)$, and the subsequent time-evolution has been probed by either one photon ionization at 197 nm or two-photon ionization at 395 nm. The decay of the optically-prepared S_1 character and the corresponding formation of the T_1 character were clearly observed in both probing schemes. The photoelectron kinetic energy distribution in (1+1') ionization exhibited clear vibrational structure that is essentially determined by Franck-Condon factors between the S_1 and cationic state. For any of the S_1 vibronic levels up to the excess energy of 2000 cm^{-1}, no signature of IVR has been observed in the photoelectron images. On the other hand, (1+2') ionization provided a few sharp lines in the kinetic energy distribution due to the accidental resonance with the 3s and 3p Rydberg states at (1+1') energy. The photoelectron angular distribution in (1+2') ionization exhibited high anisotropy, which proves that the atomic-like electron orbital is involved in the resonant state.

III-H Crossed Beam Studies on Bimolecular Reaction Dynamics

Chemical reactions under thermal conditions occur with various collision energies, internal quantum states, and impact parameters. The experimental data measured under such conditions are highly-averaged quantities, from which detailed feature of reactions can hardly be learned. A crossed molecular beam method allows us to observe chemical reactions of state-selected reagents at well-defined collision energy. Although, this method does not control the impact parameter in reaction, the differential cross section (angular distribution of products) reveals impact-parameter dependence of reaction probability and reaction mechanism. Conventional crossed beam experiments have employed so-called a universal detector (electron bombardment + quadrupole mass analysis + time-of-flight measurements). However, this method provides poor (or no) internal state resolution of products. The internal motions (electronic, vibrational and rotational) of molecules play essential roles in chemical reactions, therefore the measurements of only the scattering distributions are generally insufficient for elucidation of reaction mechanism. We constructed a new crossed beam apparatus with a high-resolution ion imaging detector. The products are state-selectively ionized by resonantly enhanced multiphoton ionization (REMPI) and their scattering distributions are directly visualized by an imaging method. The state-selective detection diminishes the signal intensity, but this is compensated by simultaneous observation of all the scattering angle. A preliminary experiment on the inelastic scattering of NO with Ar achieved the data acquisition more than two orders of magnitude faster than previous methods. A photolytic $O(^1D)$ atomic beam source has also been constructed to study stratospheric chemistry at the state-to-state differential cross section level.

III-H-1 State-Resolved Differential Cross Section Measurements for the Inelastic Scattering of NO + Ar

KOHGUCHI, Hiroshi; SUZUKI, Toshinori

The state-resolved differential cross sections (SR-DCS) of the inelastic scattering NO (j" = 0.5, Ω" = 1/2) + Ar $\rightarrow$ NO (j', Ω' = 1/2, 3/2) + Ar at 63 meV were measured by a crossed molecular beam ion-imaging method. The dynamics of this system occurs on the two potential energy surfaces that arise from the approach of Ar to NO in the $^2\Pi$ state, and the average and difference potentials of these two determine the spin-orbit changing ($\Delta\Omega$ = 1) and conserving transitions ($\Delta\Omega$ = 0). Many workers have studied NO + Ar both theoretically and experimentally as a representative system of inelastic scattering of open-shell molecules. In our experiment, twenty final (j', Ω') states in total were observed for both spin-orbit conversing (Ω" = 1/2 $\rightarrow$ Ω' = 1/2) and changing (Ω" = 1/2 $\rightarrow$ Ω' = 3/2) processes. The DCSs exhibited complex structures that are sensitive to the final (j', Ω') states; sharp forward scattering for low j' states, broad angular distributions

for intermediate *j*' states, and backward scattering for high *j*' states. The results were in excellent agreement with close-coupling calculations on the CCSD(T) surfaces performed by Millard Alexander at Maryland University.

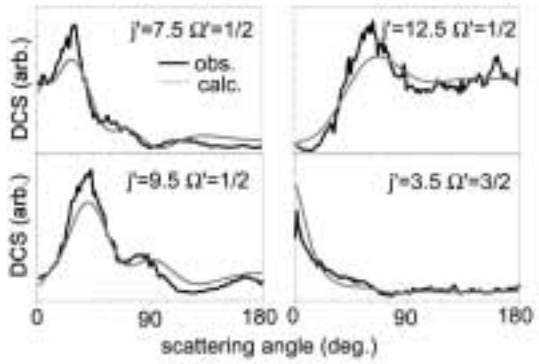

Figure 1. The observed and calculated state-resolved differential cross section of the inelastic scattering of NO + Ar. The final states of scattered NO are denoted as (*j*', Ω').

III-I Non-Adiabatic Molecular Photodissociation Dynamics Studied by Polarization Spectroscopy

Vector quantities of products provide detailed insights into the stereochemical dynamics of atomic/molecular collisions and molecular photodissociation. As expected from building-up principle of diatomic molecule, the ***orbital alignment*** and ***orientation*** in an atomic fragment carries information on the electronic symmetry of the PES. Furthermore, coherent excitation leading to two different dissociation paths creates characteristic vector correlation.

III-I-1 Atomic Orbital Orientation in Photodissociation of OCS

KATAYANAGI, Hideki; SUZUKI, Toshinori

The orbital orientation of $S(^1D_2)$ was detected in photodissociation of OCS by an ion imaging technique with circularly-polarized probe light. One of the causes for orientation is quantum mechanical interference between the two different dissociation pathways reached by parallel and perpendicular transitions. The magnitude of the orientation is proportional to the asymptotic phase difference between the pathways, making the orientation to be a sensitive probe of the potential energy surfaces. The $S(^1D_2)$ products consist of two components arising from a mixed transition to $2^1A'$, $1^1A''$ and from a pure parallel transition to $2^1A'$. The former appears with high translational energy of 12.7 kcal/mol and the latter 3.8 kcal/mol. As shown in Figure 1, the signal of high energy component showed strong orientation.

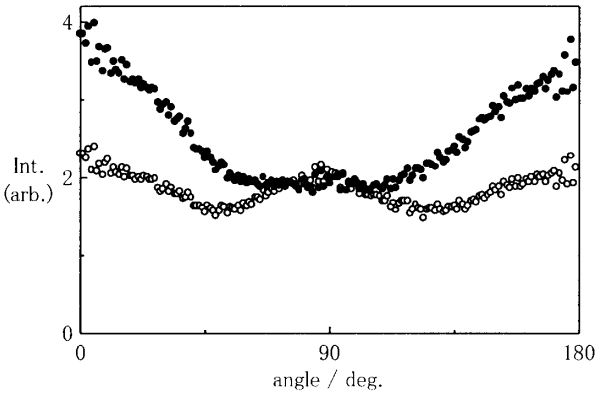

Figure 1. Angular distributions of high and low energy S^+ ions created by linearly polarized 235 nm pump light, and the right (●) left (○) circularly polarized probe light. Definition of θ is illustrated in the figure. ε_{dis} and s_{pr} are polarization vectors of the pump light and a helicity vector of the probe, respectively.

III-J Photochemistry on Well-Defined Surfaces

Upon the irradiation of light in the wavelength range from visible to ultraviolet, a number of adsorbed molecules on metal surfaces reveal variety of photochemical processes, including photo-stimulated desorption, rearrangement of adsorbed states, photodissociation, and photo-initiated reactions with coadsorbates. A central and fundamental question in the surface photochemistry is to clarify how adsorbate-substrate systems are excited by photon irradiation. In addition, since photo-initiated reactions can be induced without any thermal activation of reactants, they may provide good opportunities for studying a new class of surface reactions which may not be induced thermally. We have studied photochemistry of various adsorption systems on well-defined metal and semiconductor surfaces mainly by temperature-programmed desorption (TPD), x-ray photoelectron spectroscopy (XPS), work function measurements, and angular-resolved time-of-flight (TOF) spectroscopy of photodesorbed species associated with pulsed laser irradiation. We have shown that methane weakly adsorbed on Pt(111), Pd(111) and Cu(111) is dissociated or desorbed by irradiation of 6.4-eV photons, which is far below the excitation energy for the first optically allowed transition of methane in the gas phase. We have found that rare gas atoms are also photodesorbed from clean and modified Si(100) surfaces. These are all physisorbed systems where electronic states of adsorbate and substrate are well separated in the ground state. In contrast, we have extended the project to photochemistry of strongly chemisorbed, or compound systems on metal surfaces: AgO chains on an Ag(110) surface.

III-J-1 Excitation Mechanisms and Photochemistry of Adsorbates with Spherical Symmetry

WATANABE, Kazuo; MATSUMOTO, Yoshiyasu

[*Faraday Discuss.* **117**, 207 (2000)]

By comparing the photo-stimulated desorption of Xe from an oxidized Si(100) surface with the photochemistry of methane on metal surfaces, we try to deduce a common concept in the excited state and the excitation mechanism responsible for the photo-induced processes. Xe atoms are desorbed from the oxidized Si(100) surface by the irradiation of photons in the range of 1.16–6.43 eV. The two velocity components with average kinetic energy of 0.85 eV and 0.25 eV are observed in the time-of-fight distributions. The fast component appears only if the photon energy exceeds ~3 eV, but the slow component does in the entire photon energy range. By analogy with the photochemistry of methane on the metal surfaces, the excitation mechanism responsible for the fast component is postulated to be a transition from the 5p state of Xe to the excited state originating in strong hybridization between the 6s-state of Xe and the dangling bond at a surface silicon atom bonded with oxygen inserted in the dimer bond. In this scheme an excited electron is transferred from the adsorbate to the substrate, which is the reverse direction compared with the substrate-mediated excitation frequently assumed in surface photochemistry.

III-J-2 Photo-induced Oxygen Elimination Reaction at an Ag(110)-p(2×1)-O Surface

OTA, Michiharu[1]; WATANABE, Kazuya; MATSUMOTO, Yoshiyasu
([1]GUAS)

When an Ag(110) surface is extensively exposed to oxygen gas, well-ordered AgO chains are formed on the surface. It has been reported that oxygen atoms in the chains are eliminated by UV photon irradiation. However, the excitation mechanism for the photoreaction is completely unknown. Furthermore, there is no information on how oxygen is eliminated and where it goes. We try to uncover these questions by using LEED, XPS, TOF and TPD measurements. After confirming a characteristic LEED pattern of the Ag(110)- p(2×1)-O surface, the surface is irradiated by UV light. The depletion of the oxygen coverage is measured by post-irradiation XPS as a function of the irradiated photon numbers. The most important finding in the photoreaction is that the cross-sections for the photochemical oxygen elimination reaction strongly depend on the coverage of carbon atoms remained at the surface; the cross-section increases with the coverage of carbon atoms. Interestingly, carefully designed experiments show that carbon atoms believed to be at subsurface are more effective than carbon adatoms on the surface. Photodesorbed species are detected by a quadruple mass spectrometer. No oxygen atoms/molecules are detected, but only CO_2 molecules are detected. Therefore, subsurface carbon plays an important role in the reaction. We tentatively assign the subsurface carbon is carbidic and the carbon adatoms is graphitic. Further characterization of the carbon atoms are underway.

Reference

1) Y. Matsumoto, Y. Okawa, K. Suzuki, K. Mukai and K. Tanaka, *J. Am. Chem. Soc.* **118**, 9676 (1996).

III-K Structure and Properties of Polyoxometalates with a Magnetic, Electronic, or Biological Significance

Polyoxometalates constitute model systems for the study of the electron and energy transfer in the infinite metal-oxide lattice and their simplicity allows to treat at the molecular scale the coupling of electronic and nuclear movements, which is an inherent problem for the mixed-valence systems. As is clear from such a variety of both structure and reactivity of polyoxometalates, our current works on polyoxometalates are 1) structure/reactivity relationships with particular regard to the mechanism of electron transfer reactions, 2) magnetic interaction and molecular magnetic device, 3) energy-transfer mechanism and luminescence device (including nonlinear optical device), 4) encapsulation of templates in the photo-induced self-assembly process, 5) template-exchange reaction and topology, and 6) antibacterial effects on MRSA and VRE.

III-K-1 Luminescence and Energy Transfer Phenomena in Tb^{3+}/Eu^{3+}-Mixed Polyoxometallolanthanoates $K_{15}H_3[Tb_{1.4}Eu_{1.6}(H_2O)_3(SbW_9O_{33})(W_5O_{18})_3]\cdot 25.5H_2O$ and $Na_7H_{19}[Tb_{4.3}Eu_{1.7}O_2(OH)_6(H_2O)_6Al_2(Nb_6O_{19})_5]\cdot 47H_2O$

YAMASE, Toshihiro; NARUKE, Haruo
(IMS and Tokyo Inst. Tech.)

[*J. Phys. Chem. B* **103**, 8850 (1999)]

The energy dissipation of Tb^{3+}/Eu^{3+} cations in both heterolanthanide-multinuclear polyoxometalates, $K_{15}H_3[Tb_{1.4}Eu_{1.6}(H_2O)_3(SbW_9O_{33})(W_5O_{18})_3]\cdot 25.5H_2O$ and $Na_7H_{19}[Tb_{4.3}Eu_{1.7}O_2(OH)_6(H_2O)_6Al_2(Nb_6O_{19})_5]\cdot 47H_2O$ is studied by crystal structures, emission and excitation spectra, and emission decay dynamics. The excitation of the Tb^{3+} $^7F_6{}^5 \rightarrow D_4$ transitions produces not only the emission lines of Tb^{3+}, but also those of Eu^{3+}, accompanied by nonexponential rise and decay curves of the emission from Tb^{3+} and Eu^{3+}. There is no significant exchange interaction between the lanthanide ions, as a result of the coordination of aqua and/or hydroxo ligands to the lantahanide ions. The mechanism of the $Tb^{3+} \rightarrow Eu^{3+}$ energy transfer is identified as a Föster-Dexter-type energy transfer from Tb^{3+} (donor) to Eu^{3+} (acceptor). At low temperatures $^5D_4$(Tb) + $^7F_0$(Eu) $\rightarrow$ $^7F_4$(Tb) + $^5D_0$(Eu) governs the transfer process and at high temperatures it is governed by $^5D_4$(Tb) + $^7F_1$(Eu) $\rightarrow$ $^7F_5$(Tb) + $^5D_1$(Eu), $^5D_4$(Tb) + $^7F_1$(Eu) $\rightarrow$ $^7F_4$(Tb) + $^5D_0$(Eu), and $^5D_4$(Tb) + $^7F_2$(Eu) $\rightarrow$ $^7F_5$(Tb) + $^5D_1$(Eu) interactions which involve the thermally populated $^7F_1$ and $^7F_2$ levels. The nearest-neighbor energy-transfer rates by electric dipole-dipole interactions between a Tb-Eu pair at 4.2 K are estimated to be 4.5×10^4 and 4.7×10^5 s^{-1}, and the critical radii at 4.2 K are 10.3 and 10.0 Å for $K_{15}H_3[Tb_{1.4}Eu_{1.6}(H_2O)_3(SbW_9O_{33})(W_5O_{18})_3]\cdot 25.5H_2O$ (with Tb–Eu separation of 5.05 Å) and $Na_7H_{19}[Tb_{4.3}Eu_{1.7}O_2(OH)_6(H_2O)_6Al_2(Nb_6O_{19})_5]\cdot 47H_2O$ (with 3.76 Å separation), respectively. The low symmetry (C_s for the former and C_1 for the latter) of the LnO_8 (Ln = Tb and Eu) coordination polyhedra allows the nonvanishing electric-dipole transition probability for the $^7F_J \longleftrightarrow {}^5D_0$ (J = 0, 1) transitions which leads to a faster transfer rate at high temperatures.

III-K-2 Mixed-Valence Ammonium Trivanadate with a Tunnel Structure Prepared by Pyrolysis of Polyoxovanadate

NARUKE, Haruo; YAMASE, Toshihiro
(IMS and Tokyo Inst. Tech.)

[*Bull. Chem. Soc. Jpn.* **72**, 2699 (1999)]

The pyrolysis of a polyoxovanadate solid, $(NH_4)_{12}[V_{18}O_{42}(H_2O)]\cdot nH_2O$ ($n \approx 11$), at 300 °C in an Ar + NH_3 atmosphere gave a mixed-valence vanadium oxide, $(NH_4)_xV_3O_7$ ($x \approx 0.6$), isostructural with $Cs_{0.37}V_3O_7$. The crystal structure of $(NH_4)_xV_3O_7$ was refined by the Rietveld method (hexagonal, P63/m, a = 9.8436(6), c = 3.6165(1) Å, V = 303.47(3) Å^3, Z = 2). $(NH_4)_xV_3O_7$ comprises edge- and corner-sharing $V^{IV/V}O_5$ square-pyramids with an approximate ratio of $V^{IV}:V^V \approx 0.49:0.51$, to form a columnar cavity along the c-axis, in which ammonium N atoms are hydrogen-bonded to apical O atoms of the $V^{IV/V}O_5$ square-pyramids. A reflux of the $(NH_4)_xV_3O_7$ powder in a 0.6 M LiOH / 2-methoxyethanol solution brought about Li-insertion into the columnar cavity without any structural change in the $\{V_3O_7\}$ framework.

III-K-3 Photoassisted Dehalogenation of Organo-Chlorine Compounds by Paratungstate A in Aqueous Solutions

HU, Changwen; YUE, Bin; YAMASE, Toshihiro
(IMS and Tokyo Inst. Tech.)

[*Appl. Catal., A* **194-195**, 99 (2000)]

Nearly neutral aqueous solutions of 22 organo-chlorine compounds undergo photodegradation ($\lambda > 250$ nm) catalyzed by paratunstate A anion, $[W_7O_{24}]^{6-}$, which was obtained by adjusting pH levels of the Na_2WO_4 solution to 6–7. In each case the organic substrate was decomposed through dehalogenation. The rate of Cl^- formation strongly depends on substrates. The photochemical redox reaction between paratungstate A and substrates proceeds via precomplexation. The Langmuir-type dependence of the reaction rates on the concentration of substrates provides a promising method for the dechlorination of alkyl- and aromatic-chloride compounds such as $ClCH_2CH_2CH_2Cl$, C_3H_7Cl, and $C_6H_5CH_2Cl$.

III-K-4 A Novel-Type Mixed-ligand Polyoxotungstolanthanoate, $[Ln(W_5O_{18})(BW_{11}O_{39})]^{12-}$ (Ln = Ce^{3+} and Eu^{3+})

NARUKE, Haruo; YAMASE, Toshihiro

(IMS and Tokyo Inst. Tech.) 177 (2000)]

[*Bull. Chem. Soc. Jpn.* **73**, 375 (2000)]

Two isostructural anions, $[Ln(BW_{11}O_{39})(W_5O_{18})]^{12-}$ (Ln = Ce and Eu), were isolated as K^+ salts from aqueous solutions containing tungstate, Ln^{3+}, and BO_3^{3-}, at pH = 7. An X-ray crystallographic analysis showed that the Ln^{3+} center in the anion is chelated by two kinds of tetradentate polyoxotungstate ligands, $[W_5O_{18}]^{6-}$ and α-$[BW_{11}O_{39}]^{9-}$ with a square antiprismatic LnO_8 configuration, which are monovacant derivatives of $[W_6O_{19}]^{2-}$ and α-$[BW_{12}O_{40}]^{5-}$, respectively. The anion is of approximate C_s symmetry, and the observable asymmetry of K–O bonding between two different K^+ cations and the anion causes the two mirror planes within $[(W_5O_{18})Ln]^{3-}$ and $[(BW_{11}O_{39})Ln]^{6-}$ moieties to be canted to each other by 5.2° for Ln = Ce and 4.1° for Ln = Eu.

III-K-5 Photoreduction Processes of α-Dodecamolybdophosphate, α-$[PMo_{12}O_{40}]^{3-}$: ^{31}P-NMR, Electrical Conductivitiy, and Crystallographic Studies

ISHIKAWA, Eri; YAMASE, Toshihiro
(IMS and Tokyo Inst. Tech.)

[*Bull. Chem. Soc. Jpn.* **73**, 641 (2000)]

The photoreduction processes of α-$[PMo_{12}O_{40}]^{3-}$ (α-PMo_{12}(0)) in aqueous solutions at pH 2.0 are discussed on the basis of the results of the electrical conductivities and ^{31}P NMR spectra of photolytes, and the crystal structures of α-type two-electron and β-type four-electron reduction species isolated from photolytes as α-$[(^iPr)_2NH_2]_4[HPMo_{12}O_{40}]\cdot 4H_2O$ (**1**) (α-PMo_{12}(II)) and β-$[(^iPr)_2NH_2]_3[H_4PMo_{12}O_{40}]\cdot 2H_2O$ (**2**) (β-PMo_{12}(IV)): (i) A one-electron reduction species produced by the photoredox reaction of α-PMo_{12}(0) with methanol is degraded to α-B-$[H_3PMo_9O_{31}(OH)_3]^{3-}$ (α-B-PMo_9(0)) and Mo^V-containing Mo-triad species (Mo_3). (ii) The formation of the α-type monoprotonated two-electron reduction species, α-$[HPMo_{12}O_{40}]^{4-}$ (α-PMo_{12}(II)), results from the isomerization of the β-type two-electron reduction species, β-$[PMo_{12}O_{40}]^{5-}$ (β-PMo_{12}(II)), which is produced by coupling between the one-electron reduced α-B-PMo_9 (α-B-PMo_9(I)) and Mo_3. (iii) The β-type four-protonated four-electron reduction species, β-$[H_4PMo_{12}O_{40}]^{3-}$ (β-PMo_{12}(IV)) as a final product is produced by the disproportionation of α-PMo_{12}(II). The change in the electrical conductivity of the photolytes during photolysis supports the above processes for the photoreduction of α-$[PMo_{12}O_{40}]^{3-}$ to β-$[H_4PMo_{12}O_{40}]^{3-}$ at pH 2.0.

III-K-6 $Na_{10}(glycine)_2[H_2W_{12}O_{42}]\cdot 28H_2O$

NARUKE, Haruo; FUKUDA, Norio; YAMASE, Toshihiro
(IMS and Tokyo Inst. Tech.)

[*Acta Crystallogr., Sect. C: Cryst. Struct. Commun.* **56**,

The title compound, decasodium diglycine dihydrogendotetracontaoxododecatungstate(10-) octacosahydrate, consists of a paratungstate $[H_2W_{12}O_{42}]^{10-}$ anion, ten Na^+ cations, two zwitterionoic glycine molecules, and 28 crystallization waters. Two glycine-carboxylate O atoms coordinate three different Na^+ cations and the amino N atom forms hydrogen bonds with both terminal and bridging O atoms, two atoms for each.

III-K-7 Crystal and Electronic Structure and Magnetic Susceptibility of the Photochemically Prepared Layered Vanadyl Phosphate, $Na(VO)_2(PO_4)_2\cdot 4H_2O$

YAMASE, Toshihiro; MAKINO, Haruyo
(IMS and Tokyo Inst. Tech.)

[*J. Chem. Soc., Dalton Trans.* 1143 (2000)]

Prolonged photolysis of the aqueous solutions containing Na_3VO_4, NaH_2PO_4, and MeOH at pH 1.8 adjusted by use of H_3PO_4 led to the formation of a layered vanadyl phosphate, $Na(VO)_2(PO_4)_2\cdot 4H_2O$ (**1**). A single-crystal X-ray structural analysis of dark green crystal of **1** showed that the structure contains layers of vanadium (randomly with 1:1 ratio of V^{4+} and V^{5+}) phosphorus oxide with the water molecules and sodium cations between the layers. The layer is a 4-connected net in which corner-sharing vanadium oxygen octahedra and phosphate tetrahedra alternate. The molecular structure is identical with that of hydrothermally prepared Na^+-compound but reveals the nonzero dihedral angle (2.61°) between the least-square planes (containing equatorial four-oxygen atoms) of the VO_6 octahedra in contrast to the parallel arrangement of the basal least-square planes for the latter. Magnetic susceptibility measurements for **1** show weak ferromagnetic coupling (J/k = 0.87 K) at $T \leq 100$ K and weak antiferromagnetic behavior at $T > 100$ K. The magneto/structural relationship for the retracted-chair-like $V(OPO)_2V$ rings are compared among other layered vanadyl phosphate compounds. The ferromagnetic property of the d_{xy} orbital at one V^{IV} center in the retracted-chaired $V^{IV}(OPO)_2V^{IV}$ ring can be explained in terms of the interaction with the V=O π* orbital at opposite V^{IV} center, which is possible when both distances of (O=)V··V(=O) and (O=)V··O(=V) are short (~4.55 and ~4.36 Å, respectively). Otherwise, the antiferromagnetic property due to the superexchange interaction between magnetic d_{xy} orbitals at both V^{IV} centers is operative. The results of Extended Hückel (EH) calculations for a fragment model $[V_8P_8O_{40}]^{4-}$ (with V^{IV}/V^V = 1/1) support a variety of the magnetic interaction of the unpaired electron at V^{IV} centers in the V–P–O layer consisting of the retracted-chaired $V(OPO)_2V$ rings.